JPE 19-5-20

https://doi.org/10.6113/JPE.2019.19.5.1270
ISSN(Print): 1598-2092 / ISSN(Online): 2093-4718

Control Strategy and Stability Analysis of Virtual Synchronous Generators Combined with Photovoltaic Dynamic Characteristics

Xiying Ding*, Tianxiang Lan†, and Henan Dong**

†,*Shenyang University of Technology, Shenyang, China
**Liaoning Electric Power Company Electric Power Research Institute,
State Grid Corporation of China, Shenyang, China

Abstract

A problem with virtual synchronous generator (VSG) systems is that they are difficult to operate stably with photovoltaic (PV) power as the DC side. With this problem in mind, a PV-VSG control strategy considering the dynamic characteristics of the DC side is proposed after an in-depth analysis of the dynamic characteristics of photovoltaic power with a parallel energy-storage capacitor. The proposed PV-VSG automatically introduces DC side voltage control for the VSG when the PV enters into an unstable working interval, which avoids the phenomenon where an inverter fails to work due to a DC voltage sag. The stability of the original VSG and the proposed PV-VSG were compared by a root locus analysis. It is found that the stability of the PV-VSG is more sensitive to the inertia coefficient J than the VSG, and that a serious power oscillation may occur. According to this, a new rotor model is designed to make the inertial coefficient automatically change to adapt to the operating state. Experimental results show that the PV-VSG control strategy can achieve stable operation and maximum power output when the PV output power is insufficient.

Key words: Photovoltaic, Output power oscillation, Stability analysis, Virtual synchronous generator

I. INTRODUCTION

As a kind of inverter control technology that can participate in primary frequency regulation and provide a certain inertia to the power grid, a virtual synchronous generator (VSG) provides a new development direction for the grid-connection of large-scale distributed photovoltaic (PV) power [1]-[4]. However, in the current research related to VSGs, most scholars focus on the VSG control itself, and the DC side is replaced by an ideal voltage source. Some scholars study the VSG system with an energy-storage battery as the DC side [5], [6]. Neither of these approaches solve the grid-connection problem of actual PVs, and they both largely ignore the influence of the dynamic characteristics of the DC side. In fact, the output of a distributed PV power supply is susceptible to external environmental factors, and there are problems such as stable operation intervals and capacity limitations [7]. If the traditional VSG control is adopted, it is easy to make the output power of the VSG higher than the output limit of the PV, which may result in an inverter failure [8].

In view of the above problems, many scholars have conducted relevant research. Arco and his coworkers [9] proposed a state space model of a VSG and conducted a stability analysis. They also revealed the relationship between different control parameters and the stability of the VSG. However, the DC side was replaced by an ideal voltage source, so whether a fluctuation of the DC side voltage would affect its stability was not considered. Liu [10] pointed out the difficulties and possible problems of VSG control when compared with droop control. They also explained the cause of power oscillations of VSGs. Xin [11] proposed a droop control using PV as the DC side. However, it was an open-loop control for output

Manuscript received Mar. 11, 2019; accepted May 29, 2019
Recommended for publication by Associate Editor N. Prabaharan.
†Corresponding Author: 13591541801@163.com
Tel: +86-13591541801, Shenyang University of Technology
*Shenyang University of Technology, China
**Liaoning Electric Power Company Electric Power Research Institute, State Grid Corporation of China, China

power. Zhang [12] and Torres [13] proposed VSG-based PV grid-connection control schemes, and focused on the study of energy storage devices and primary frequency modulation performance. However, for a VSG, its DC side is still an ideal voltage source, and a large energy storage battery needs to be configured. Alipoor [14] proposed an inertial adaptive control strategy to solve the power oscillation problem. They also provided a theoretical basis for changing the parameters while the VSG is running. However, this method does not solve the grid-connection problem of PVs. Although scholars have done a lot of research on the VSG itself, there has been no research on a PV's stable grid-connection through a VSG.

In order to make a VSG that takes a PV as a source stable, the dynamic characteristics of the DC side need to be fully considered. In view of this, a PV-VSG with an additional DC voltage control is proposed in this paper, which can effectively restraint the DC voltage sag caused by an energy shortage. Then, by comparing the stability of an original VSG with the proposed PV-VSG, it can be concluded that the proposed strategy makes the system stability more susceptible to the coefficient J, which can result in power oscillation. For this reason, a new rotor model is designed to automatically change the inertia value during operation.

II. Analysis of the PV-VSG Structure and the Dynamic Characteristics of the DC Side

Unlike traditional VSG systems that take a DC voltage source as the source side, the PV-VSG uses a combination of a PV and a capacitor as the virtual prime mover. This combination has more complex dynamic characteristics, and is fundamentally different from the traditional VSG system with its energy-storage battery [15].

The internal structure of a PV is complex. In order to simplify the analysis on its operating principle, the stable operation interval and unstable operation interval are defined in the *P-U* curve shown in Fig. 1 [13]. The horizontal axis is the terminal voltage of the PV, and the vertical axis is the available power of the PV; ($U_{dc\text{-}mpp}$, P_{mpp}) is the maximum power output point (MPP) of the PV; U_{oc} is the maximum voltage of the PV; and P_{load} is the power required by the load. Among the intervals, II is the stable operation interval, and I is the unstable operation interval. If the power shared by the PV-VSG is greater than that of P_{mpp}, as shown in the figure, the PV enters interval I. With an increase of P_{load}, U_{dc} decreases, which results in a decrease in the output power of the PV. This vicious circle causes the voltage to drop rapidly to a collapse of the inverter.

In the PV-VSG, the DC voltage does not drop rapidly when P_{load} is greater than P_{mpp} due to the presence of a parallel capacitor. Its dropping rate depends on the capacity of the parallel capacitor.

For the parallel capacitor:

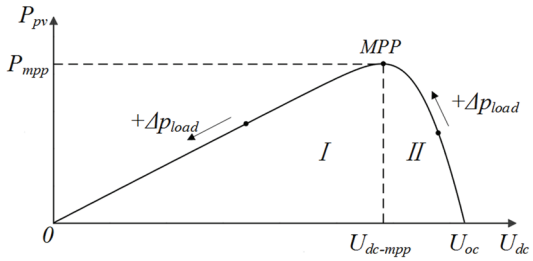

Fig. 1. Operation interval of a photovoltaic power supply.

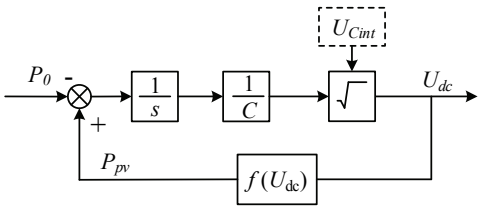

Fig. 2. DC side equivalent model.

$$\Delta Q = \Delta U_C C \tag{1}$$

Where ΔQ is the electric charge in the capacitor, ΔU is the voltage of the capacitor, and C is the capacity of the capacitor.

$$\Delta Q \Delta U_C = \Delta W = \int_0^t (P_0 - P_{pv}) \mathrm{d}t \tag{2}$$

Where P_0 is the discharge power of the capacitor and ΔW is the discharge energy of the capacitor in time t. Combining Equation (1) with Equation (2), the value of the DC side voltage is obtained:

$$U_{dc} = U_{Cint} \pm \sqrt{\frac{\int_0^t \left| P_{pv} - P_0 \right| \mathrm{d}t}{C}} \quad P_{pv} \gtrless P_0 \tag{3}$$

U_{Cint} is the initial voltage value of the capacitor; and P_{pv} is a function of U_{dc}, that is $f(U_{dc})$, which is described by a P-U curve of the PV. In order to simplify the small signal analysis in the following part, linearization fitting is done for the P-U curve around the MPP. Therefore:

$$P_{pv} = \begin{cases} \dfrac{P_{mpp}}{U_{dc-mpp}} U_{dc} & U_{dc} \in \mathrm{I} \\ -\dfrac{P_{mpp}}{U_{oc} - U_{dc-mpp}} U_{dc} + \dfrac{U_{oc} P_{mpp}}{U_{oc} - U_{dc-mpp}} & U_{dc} \in \mathrm{II} \end{cases} \tag{4}$$

An equivalent model of the PV and the capacitor can be obtained from Equation (3) and Equation (4), as shown in Fig. 2.

According to Fig. 2, when the load increase from P_{mpp}, the variation trend of U_{dc} is as shown in Fig. 3. U_{dmin} is the minimum voltage of the DC side, which keeps the inverter working normally.

As shown in Fig. 3, the design of the capacitor should meet the condition that the DC side voltage is no less than U_{dmin}, which may result in inverter failure under a temporary load

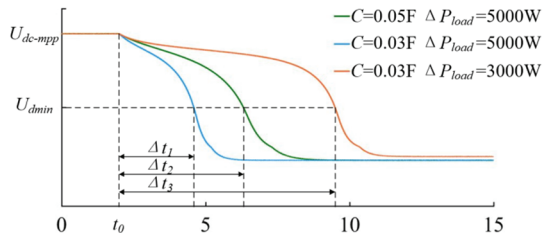

Fig. 3. Simulation result of DC-terminal voltage under a DC terminal equivalent model.

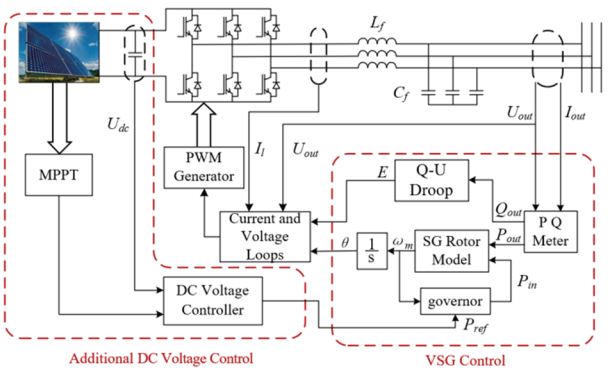

Fig. 4. Block diagram of the proposed PV-VSG control.

fluctuation in a certain time range Δt. However, the actual quantity and duration of ΔP_{load} cannot be predicted, and the capacity of capacitor cannot be designed to be infinite. There is always a risk of using up the energy in the capacitor. In addition to the increase of the load, the PV itself can also have an impact on the supply-demand relationship of the power. These impacts can include changes in the intensity of illumination, changes in the environmental temperature and local malfunctions. Therefore, in the control of the PV-VSG, both the change of load and the working status of the PV itself should be considered with a MPPT device.

It is worth mentioning that MPPT is generally divided into two methods: the closed-loop method and the open-loop method. When compared with the open-loop method, the closed-loop method requires the inverter to work at the maximum power point, which means that the VSG loses the abilities of frequency and voltage regulation. In fact, to prevent the PV from entering the unstable interval, only the parameter Udc-mpp is necessary. Therefore, the constant voltage tracking method is selected in this paper. The effect of temperature on the Udc-mpp is ignored.

III. PV-VSG Control Strategy with DC Side Voltage Control

Due to the non-monotonic relationship of PV power-voltage, DC voltage sag may occur if the traditional VSG control strategy is used. Therefore, this paper proposes a VSG control strategy with additional DC side voltage control. The overall modeling is shown in Fig. 4, which can be divided into two parts: VSG control and an additional DC voltage control.

A. Control Strategy of a VSG

Since this paper focuses on the transmission and control of active power, as shown in Fig. 4, the reactive power control part of the VSG ontology only adopts the *Q-U* droop controller as the droop control, which is not discussed in this paper. The active power control part simulates the rotor model and governor model of the synchronous generator (SG) [16]-[18]. The SG rotor model can be expressed as follows:

$$P_{in} - P_{out} = J\frac{\mathrm{d}\omega_m}{\mathrm{d}t} + D_p(\omega_m - \omega_g) \tag{5}$$

Where J is the rotary inertia of the rotor, ω_m is the angular frequency of the rotor, D_p is the damping coefficient, and ω_g is the angular frequency measured from the VSG output port. P_{in} is the input power of the rotor, which is the instruction power calculated in the virtual governor in the VSG; and P_{out} is the output power of the rotor, which is the output power measured from inverter in the VSG. The SG rotor model shown in formula (5) simulates the two most important links in the SG: the inertia and damping. This makes the SG superior to a grid-connected inverter. In [10], ω_g is replaced by a constant value because the measurement of ω_g has a certain time delay. As a result, (5) becomes:

$$P_{in} - P_{out} = J\frac{\mathrm{d}\omega_m}{\mathrm{d}t} + D_p(\omega_m - \omega_{ref}) \tag{6}$$

Where ω_{ref} is the reference value of the angular frequency. The governor model in Fig. 4 can be written as:

$$P_{in} = (\omega_{ref} - \omega_m)K_\omega + P_{ref} \tag{7}$$

P_{ref} is the active power reference value of the VSG; and K_ω is the droop coefficient. It can be seen that the process shown in (6) is similar to the primary frequency modulation of the SG. At this point, the governor is the same as the *P-ω* droop controller. According to (6) and (7), the VSG is actually a droop control with additional inertia and damping functions.

Combining (6) and (7) yields:

$$P_{ref} - P_{out} = J\frac{\mathrm{d}\omega_m}{\mathrm{d}t} + (K_\omega + D_p)(\omega_m - \omega_{ref}) \tag{8}$$

It can be seen that the damping term and the droop term have the same effect and are directly proportional to $(K_\omega + D_p)$. Although this solution improves the droop coefficient of the frequency, which can affect the power distribution in the steady-state, it also increases the damping ratio and can reduce the phenomenon of output power oscillation [8]. It is worth mentioning that virtual impedance control has been included in the current and voltage loops in order to eliminate the influence of the line impedance on the control system.

B. Additional DC Voltage Control

According to the analysis in Chapter 2, the DC voltage $U_{dc\text{-}mpp}$ corresponding to the MPP point is the minimum DC

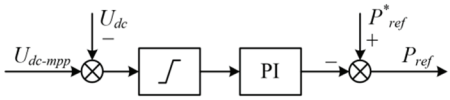

Fig. 5. Block diagram of the DC voltage controller.

voltage that can be reached by the PV in the stable interval. When the DC voltage is lower than $U_{dc\text{-}mpp}$ due to an increased load or decreased intensity of illumination, that is, when the PV enters into unstable interval I, the output power P_{out} of the VSG should be decreased, so the PV can return to the MPP working point. The additional load power can be share by other micro sources in the network.

The DC voltage controller shown in Fig. 4 is designed and added, and a block diagram of controller is shown in Fig. 5. In this figure, P^*_{ref} is the given power value; and P_{ref} is the given power value through the DC voltage controller. The lower limit of the amplitude limiting module is 0. $U_{dc\text{-}mpp}$ is the given value, and the capacitor voltage U_{dc} is the feedback value. the synthetic P_{ref} from the controller becomes the reference value of the governor.

When U_{dc} is higher than $U_{dc\text{-}mpp}$, that is, the PV enters stable Interval II, the input of the PI controller is 0 due to amplitude limiting, which means the reference value of the output power of the governor is a constant value P^*_{ref}. The VSG runs in the traditional mode. When U_{dc} is lower than $U_{dc\text{-}mpp}$, that is, the PV enters unstable Interval I, the voltage deviation synthesizes a new P_{ref} through the PI controller to reduce the reference value of the output power. It can be known from (8) that the actual output power of the VSG can be reduced. Thus, the DC side voltage rises back to $U_{dc\text{-}mpp}$, which means the PV can return to the maximum power point. In conclusion, the reference value of the output power of the governor is:

$$P_{ref} = \begin{cases} P^*_{ref} - (K_p + K_i \dfrac{1}{s})(U_{dc-mpp} - U_{dc}) & U_{dc} \in \mathrm{I} \\ P^*_{ref} & U_{dc} \in \mathrm{II} \end{cases} \tag{9}$$

Although many studies have proved that the VSG has excellent stability, it can be seen above that the DC voltage controller actually adds an extra closed loop for the VSG. Therefore, the stability of the PV-VSG needs to be re-analyzed.

IV. Stability Analysis and Method Improvement

In order to analyze the stability of the proposed PV-VSG control strategy, it is necessary to establish a small signal model of the VSG without the DC side voltage control. According to the transmission characteristics of the line [19]:

$$P_0 = \frac{EU}{X}\delta \tag{10}$$

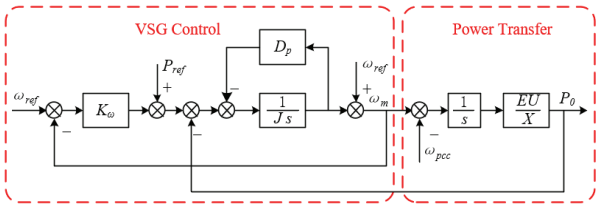

Fig. 6. Power transfer small signal model of a traditional VSG.

P_0 is the output power of the inverter, U is the voltage amplitude of the PCC point, E is the output voltage amplitude of the inverter, X is the line impedance, and δ is the phase difference between the output voltage of the inverter and the voltage of the PCC point. In addition:

$$\delta = \int_0^t \Delta\omega \mathrm{d}t = \int_0^t (\omega_m - \omega_{pcc})\mathrm{d}t \tag{11}$$

Where ω_{pcc} is the angular frequency of the PCC point. Thus, the VSG power transfer model is obtained, as shown in Fig. 6.

On the basis of Fig. 6, the PV and capacitor model shown in Fig. 2 and the control strategy shown in Fig. 5 are introduced. Thus, a power transfer small signal model of the PV-VSG with additional DC voltage control is obtained, as shown in Fig. 7.

Because an integral link is introduced because of the added DC side model, an additional pole is introduced to the characteristic equation of Fig. 7, which may bring potential instability factors to the system. In the MATLAB/Linear Analysis Tool, root locus analyses are performed in the models shown in Fig. 6 and Fig. 7, and the used parameters are shown in Table I. The results are shown in Fig. 8 and Fig. 9.

It is worth mentioning that $f(U_{dc})$ has been linearized as shown in equation (4). In addition, due to the existence of the amplitude limiting module, only when the operating point is located on the left side of MPP can it form the closed loop of the DC side as shown in Fig. 7. Thus, according to equation (4), $f(U_{dc})$ is equivalent to the proportional coefficient K.

As shown in Fig. 8, no matter how much the inertia coefficient J changes, the closed-loop pole of the system is always in the left half plane of the imaginary axis, which means that the value of J does not affect the stability of the VSG system. However, in Fig. 9, when the inertia coefficient J increases to 9.5 kgm^2, the closed-loop pole of the system enters the right half of the imaginary axis, which means that the value of J is limited when the DC side voltage closed-loop control is added to the VSG. However, reducing the inertia coefficient J for this reason undoubtedly affects the inertia performance of the system [19], [20]. In addition, the entire closed-loop pole of Fig. 9 is closer to the imaginary axis than that of Fig. 8, which means that the oscillation of the output power of the PV-VSG system is greater than that of the VSG under the same inertia coefficient J.

As pointed out in the previous chapter, the PV works at the

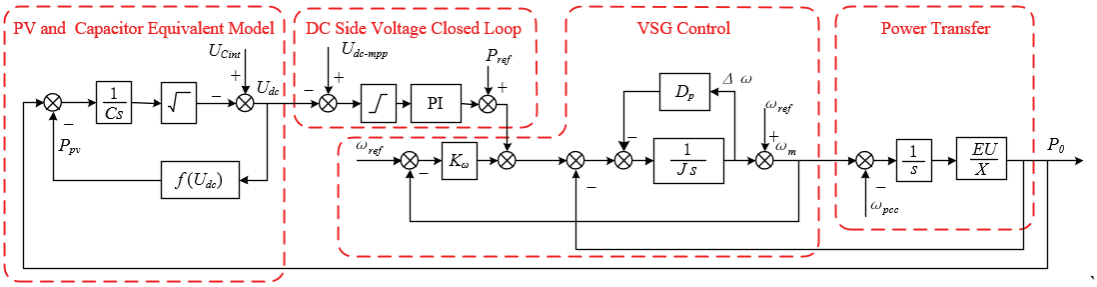

Fig. 7. Power transfer small signal model of the proposed PV-VSG.

TABLE I
PARAMETERS USED IN TOOT LOCUS ANALYSIS

Parameter	Value
Filter inductance (L_f)	0.6 mH
Filter capacitance (C_f)	0.45 mF
Line impedance resistance (R_{line})	0.0028Ω
Line impedance inductance (L_{line})	5.6 mH
Ac bus voltage (E_{bus})	380 V
Inverter output voltage (U_{dg})	380 V
AC bus angular frequency (ω_{pcc})	314 rad/s
DC side capacitance (C)	0.015 F
Reference angular frequency (ω_{ref})	314 rad/s
Droop coefficient (K_ω)	60
Damping coefficient (D_p)	20
Reference output power (P_{ref})	12 kW
DC side capacitance initial voltage (U_{Cint})	900 V
PV voltage at maximum power point ($U_{dc\text{-}mpp}$)	800 V
Proportion coefficient of PI controller (K_p)	80
Integration coefficient of PI controller (K_i)	20
Inertia coefficient of VSG (J)	1-200 kgm^2

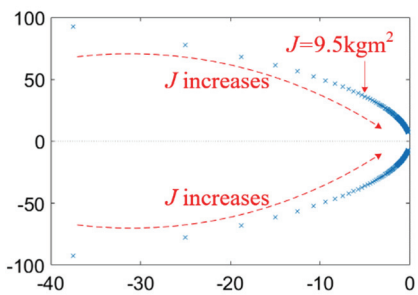

Fig. 8. Root locus analysis of a traditional VSG when the inertia coefficient J changes from 1 kgm^2 to 200 kgm^2.

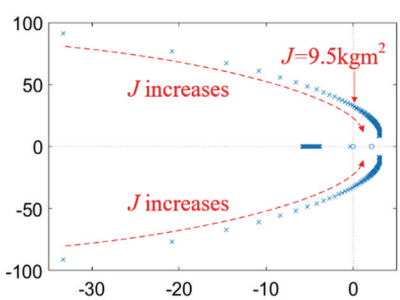

Fig. 9. Root locus analysis of the PV-VSG with DC voltage control when the inertia coefficient J changes from 1 kgm^2 to 200 kgm^2.

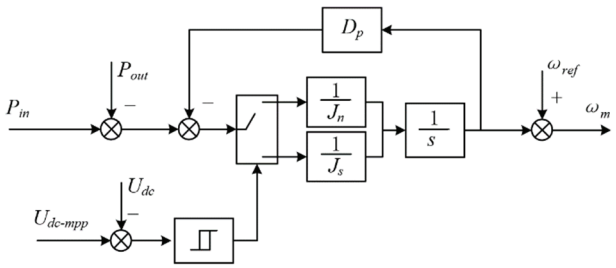

Fig. 10. Structure diagram of the improved rotor model.

MPP point when U_{dc} is less than $U_{dc\text{-}mpp}$, that is, the additional DC side voltage control takes effect, which means that the inverter output constant power does not participate in frequency modulation work at this time. At the same time, the inertia link of the VSG also loses its significance. Therefore, the inertial link can be greatly reduced when the additional DC side voltage control comes into effect to maintain the stable operation of the system.

According to this, the rotor model shown in equation 5 is improved to make the inertial coefficient automatically change according to the operating state, as shown in Fig. 10. When U_{dc} is less than $U_{dc\text{-}mpp}$, switch to the small inertia coefficient J_s; otherwise, maintain the normal inertia coefficient J_n. Because the inertia coefficient J only affects the dynamic process of the system when the frequency changes, this switching does not affect the stability of the system near the switching point. A threshold for ΔU can be applied to avoid the chattering of J during operation. This threshold is set to 3% of $U_{dc\text{-}mpp}$ in this paper.

If the improved rotor inertia coefficient is switched to J_n, the additional DC control is not introduced at this time. Then the system remains stable. If the inertia coefficient is switched to J_s when the closed loop with the additional DC control is added, the root locus of the system is still on the left side of the longitudinal axis due to switching to a smaller inertia coefficient. Therefore, stable operation of the PV-VSG is achieved.

V. EXPERIMENTAL VERIFICATION

In order to verify the feasibility of the PV-VSG control scheme, a system where two PV-VSGs are parallel with each

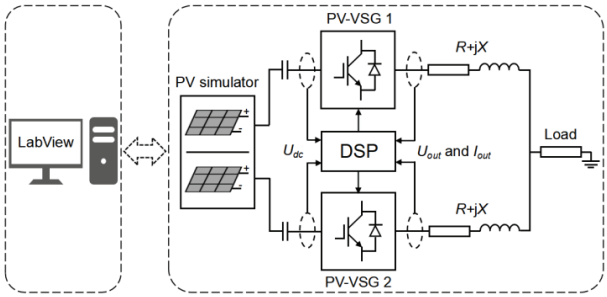

Fig. 11. Experimental system.

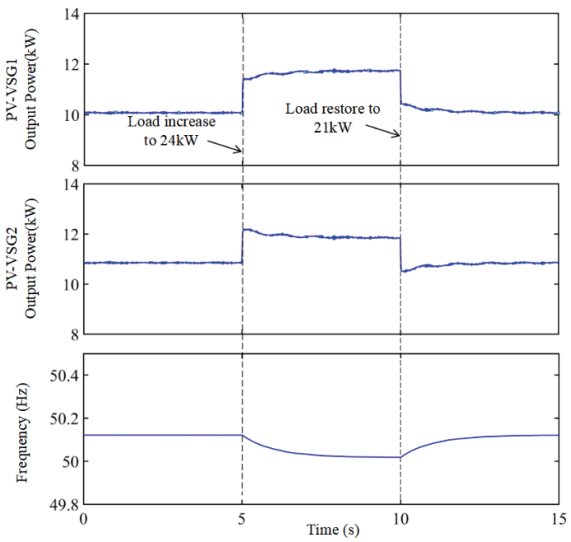

Fig. 12. Output power and frequency when power supply always exceeds the demand.

other is selected as the experimental object. The overall system configuration is shown in Fig. 11.

The outputs of the two parts of the PV simulators are independent of each other. The computer, which runs LabView, controls the PV simulator and observes the operation status of the system online. The main parameters of the system are the same as those in Table I. Two different working conditions were selected for verification.

A. Load Fluctuation under the Premise of the Power Supply Exceeding the Demand

The two PVs are always under the rated intensity of illumination I_0, and P_{mpp} is 17.5kW. The main parameters of the two VSGs are the same, and the inertia coefficient is 12 kgm^2. However, the droop coefficient of VSG2 is 40. The load is 21kW at 0s. It increases to 24kW at 5s and is restored to 21kW at 10s. The power supply always exceeds the demand. The system has been running steadily since 0s.

Since the power supply always exceed the demand, U_{dc} is always greater than $U_{dc\text{-}mpp}$, when the additional DC side voltage control was not introduced, and the PV-VSG was operated in the traditional VSG mode. As show in Fig. 12, the output powers of the two PV-VSG increase as the load

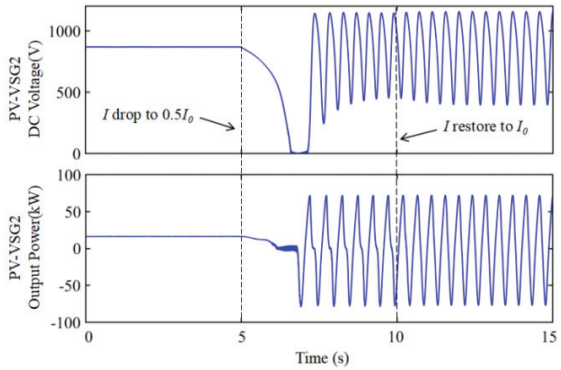

Fig. 13. DC voltage and output power of PV-VSG2 under the traditional VSG control.

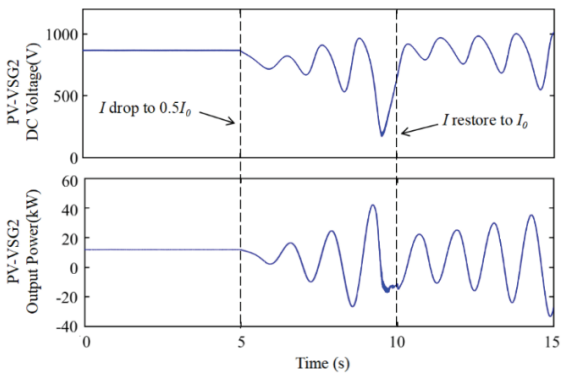

Fig. 14. DC voltage and output power of PV-VSG2 with the additional DC side voltage control.

increases and the power is shared according to the droop coefficient. However, the frequency changes slowly because both of the VSGs provide inertia for system.

B. Power Shortage Caused by a Sudden Drop in the Intensity of Illumination.

The experimental parameters are the same as those in the previous example, and the two VSGs have the same droop coefficients. The load is constant at 22kW and the intensity of illumination of PV2 changes to $0.5I_0$ at 5s and returns to I_0 at 10s. The intensity of illumination of PV1 is constant at I_0. The system has been running steadily since 0s.

Taking PV-VSG2 as example, there is no additional DC side voltage control or improved rotor model in Fig. 13. Both of the PV-VSGs run steadily before 5s. The voltage of the PV is about 850V and it operates in the stable interval. At 5s, there is a sharp drop in the intensity of illumination of PV2, P_{mpp} is reduced greatly and there is a phenomenon of short supply. The electric charge of the DC side parallel capacitor is gradually depleted resulting in a stepping down of the voltage, and the PV enters into the unstable interval. After a period of time, the DC terminal voltage is not enough to maintain the normal operation of the inverter, which leads to a collapse of the parallel system. Even when the illumination is restored at 10s, the system cannot return to the stable operation point.

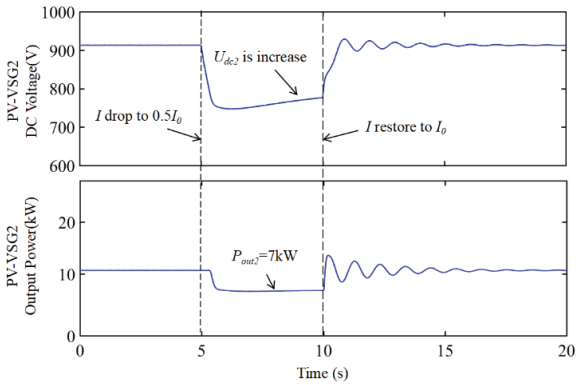

Fig. 15. DC voltage and output power of PV-VSG2 with the additional DC side voltage control and the improved rotor model.

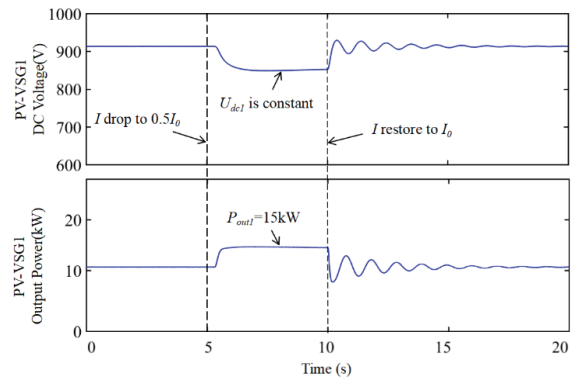

Fig. 16. DC voltage and output power of PV-VSG1 with the additional DC side voltage control and the improved rotor model.

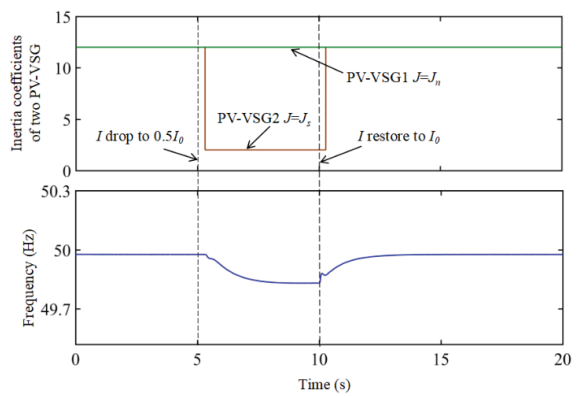

Fig. 17. Inertia coefficient and frequency with the additional DC side voltage control and the improved rotor model.

When the additional DC side voltage control is added, as shown in Fig. 14, the DC side voltage control effectively inhibits the collapse of the system caused by a sharp decline of the DC voltage. However, the stability of the system decreases after the DC side voltage control is added. It can be seen in the figure that both the DC voltage and the output power oscillate and present a diverging trend.

Due to the addition of the improved rotor model, the inertia of PV-VSG2 decreases and the stability of the system is improved when the DC side voltage control comes into effect. As shown in Fig. 15, the output power of PV-VSG2 can be stabilized at 7kW after 5s, and the DC voltage gradually rises. Because the intensity of illumination of PV1 is constant, no matter how much the control mode of PV-VSG2 changes, PV-VSG1 runs under the traditional VSG control during the whole operation process, as shown in Fig. 16. It is worth mentioning that, as can be seen from Fig. 17, the system frequency does not change quickly when the additional DC side voltage control and the improved rotor model have taken effect. This is due to the fact that the total inertia of the system is always the sum of the inertia of the two PV-VSGs.

VI. Conclusion

Since it is difficult to apply the traditional VSG to a PV connected to the grid, this paper proposes a PV-VSG system which can automatically cut into DC side voltage control when a PV is short of supply, in order to avoid the inverter failures caused by voltage sag. The results of a stability analysis on the proposed system show that the additional voltage closed loop reduces the stability of the entire system, which can cause serious power oscillation. For this reason, a new rotor model is designed to realize the switching of the inertia coefficient to improve the stability of the system. Finally, the effectiveness of the proposed control strategy and improvement measures are verified by experimental results.

References

[1] M. Guan, W. Pan, J. Zhang, Q. Hao, J. Cheng, and X. Zheng, "Synchronous generator emulation control strategy for voltage source converter (VSC) stations," *IEEE Trans. Power Syst*., Vol. 30, No. 6, pp. 3093-3101, Nov. 2015.

[2] Q. Zhong and G. Weiss, "Synchronverters: Inverters that mimic synchronous generators," *IEEE Trans. Ind. Electron*., Vol. 58, No. 4, pp. 1259-1267, Apr. 2011.

[3] J. Alipoor, Y. Miura, and T. Ise, "Stability assessment and optimization methods for microgrid with multiple VSG units," *IEEE Trans Smart Grid*, Vol. 9, No. 2, pp. 1462-1471, Mar. 2018.

[4] Q. Zhong, P. L. Nguyen, Z. Ma, and W. Sheng, "Self-synchronized synchronverters: Inverters without a dedicated synchronization unit," *IEEE Trans. Power Electron.*, Vol. 29, No. 2, pp. 617-630, Feb. 2014.

[5] J. Fang, Y. Tang, H. Li, and X. Li, "A battery/ ultracapacitor hybrid energy storage system for implementing the power management of virtual synchronous generators," *IEEE Trans. Power Electron*., Vol. 33, No. 4, pp. 2820-2824, Apr. 2017.

[6] M. Torres, L. Lopes, L. Moran, and J. Espinoza, "Self-tuning virtual synchronous machine: A control strategy for energy storage systems to support dynamic frequency control," *IEEE Trans Energy Convers.*, Vol. 29, No. 4, pp. 833-840, Dec. 2014.

[7] D. Rekioua, and E. Matagne, Optimization of Photovoltaic Power Systems: Modelization, Simulation and Control, Springer London, Chap. 2, pp. 37-64, 2012.

[8] Q. Zhong and T. Hornik, Control of Power Inverters in Renewable Energy and Smart Grid Integration, Wiley-IEEE Press, Chap. 3, 2012.
[9] S. D. Arco, J. A. Suul, and O. B. Fosso, "A virtual synchronous machine implementation for distributed control of power converters in smartgrids," *Electr. Power Syst. Res*., Vol. 122, pp. 180-197, May. 2015.
[10] J. Liu, Y. Miura, and T. Ise, "Comparison of dynamic characteristics between virtual synchronous generator and droop control in inverter-based distributed generators," *IEEE Trans. Power Electron*., Vol. 31, No. 5, pp. 3600-3611, May 2016.
[11] H. Xin, Y. Liu, Z. Wang, D. Gan, and T. Yang, "A new frequency regulation strategy for photovoltaic systems without energy storage," *IEEE Trans. Sustain. Energy*, Vol. 4, No 4, pp. 985-993, Oct. 2013.
[12] R. Zhang, H. Zhang, W, Feng, and K. Sun, "Small signal analysis of photovoltaic-energy storage integrated virtual synchronous generator," in *Proc. IEEE Ind. Eect. Soc*., pp. 1544-1549, 2017.
[13] M. Torres, C. Baier, J. M. Mauricio, and J. Silva, "Non-linear control of a grid-connected multi-cell photovoltaic inverter that operates under variable temperature and irradiance" in *Proc. IEEE Ind. Tech*., pp. 17-19, 2015.
[14] J. Alipoor, Y. Miura, and T. Ise, "Power system stabilization using virtual synchronous generator with alternating moment of inertia," *IEEE J. Emerg. Sel. Topics Power Electron*., Vol. 3, No. 2, pp. 451-458, Jun. 2015.
[15] A. Vassilakis, P. Kotsampopoulos, N. Hatziargyriou, and V. Karapanos, "A battery energy storage based virtual synchronous generator," in *Proc. IEEE, IREP Symp. Bulk Power Syst. Dyn. and Control*, pp. 25-30, 2013.
[16] J. Liu, Y. Miura, H. Bevrani, and T. Ise, "Enhanced virtual synchronous generator control for parallel inverters in microgrids," *IEEE Trans. Smart Grid*, Vol. 8, No. 5, pp. 2268-2277, Sep. 2017.
[17] H. Bevrani, T. Ise, and Y. Miura, "Virtual synchronous generators: A survey and new perspectives," *Int. J. Electr. Power Energy Syst*., Vol. 54, pp. 244-254, Jan. 2014.
[18] Y. Wei, H. Zhang, and K. Sun, "Pre-synchronization method of virtual synchronous generator using virtual power," *Autom. Electr. Power Syst*., Vol. 12, pp. 124-129, Dec. 2016.
[19] L. Huang, L. Zhang, and H. Xin, "Mechanism analysis of virtual power angle stability in droop-controlled inverters," *Autom. Electr. Power Syst*., Vol. 12, pp. 117-123, Dec. 2016.
[20] T. Shintai, Y. Miura, and T. Ise, "Oscillation damping of a distributed generator using a virtual synchronous generator," *IEEE Trans. Power Del.*, Vol. 29, No. 2, pp. 668-676, Apr. 2014.

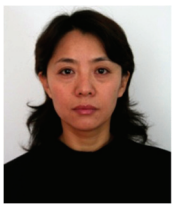

Xiying Ding was born in Shenyang, China, in 1964. She received her B.S. degree in Electrical Engineering from Northeastern University, Shenyang, China, in 1985; and her M.S. and Ph.D. degrees in Automatization Specialty from the Shenyang University of Technology, Shenyang, China, in 1987 and 2010, respectively. She has been a Professor of Electrical Engineering at the Shenyang University of Technology since 2008. Her current research interests include the running control of smart power grids.

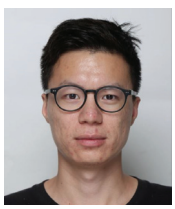

Tianxiang Lan was born in Fushun, China, in 1994. He received his B.S. degree from the Shenyang University of Technology, Shenyang, China, where he is presently working towards his M.S. degree in Electrical Engineering. His current research interests includes power system stability, photovoltaic power, and the application of new power electronic devices in power systems.

Henan Dong was born in Chifeng, China, in 1986. He received his M.S. and Ph.D. degrees in Electrical Engineering from the Shenyang University of Technology, Shenyang, China. His current research interests include the key technology and power quality of microgrids. From 2013 to 2018, he was a Senior Engineer at the Liaoning Electric Power Company Electric Power Research Institute, Liaoning, China.